ACS Photonics

Article

Cite This: ACS Photonics 2018, 5, 2129−2136

High Internal Emission Efficiency of Silicon Nanoparticles Emitting in the Visible Range

Bart van Dam,[†] Clara I. Osorio,[‡] Mark A. Hink,[§] Remmert Muller,[‡] A. Femius Koenderink,[†,‡] and Katerina Dohnalova*[,†,⊥]

[†]Institute of Physics, University of Amsterdam, Science Park 904, 1098 XH, Amsterdam, The Netherlands

[‡]Center for Nanophotonics, AMOLF, Science Park 104, 1098 XG, Amsterdam, The Netherlands

[§]Section of Molecular Cytology and van Leeuwenhoek Centre for Advanced Microscopy, Swammerdam Institute for Life Sciences, University of Amsterdam, Science Park 904, 1098 XH, Amsterdam, The Netherlands

Supporting Information

ABSTRACT: Light-emitting silicon nanoparticles (Si-NPs) are interesting for lighting applications due to their nontoxicity, chemical robustness, and photostability; however, they are not practically considered due to their low emission efficiencies. While large Si-NPs emitting in the red to infrared spectral region show ensemble emission quantum efficiencies up to 60%, the emission efficiencies of smaller Si-NPs, emitting in the visible spectral range, are far lower, typically below 10−20%. In this work, we test this efficiency limit by measuring for the first time the internal quantum efficiency (IQE), i.e., the higher bound of the emission quantum efficiency, considering only the emissive NPs within the ensemble, of Si-NPs emitting in the visible spectral range between 350 and 650 nm. On the basis of photoluminescence decay measurements in a Drexhage geometry, we show that Si-NPs with organic passivation (C:Si-NPs) can have high direct-bandgap-like radiative rates, which enable a high IQE over ∼50%. In this way, we demonstrate that Si-NPs can in principle be considered a competitive candidate as a phosphor in lighting applications and medical imaging also in the visible spectral range. Moreover, our findings show that the reason for the much lower ensemble emission efficiency is due to the fact that the ensemble consists of a low fraction of emissive NPs, most likely due to a low PL "blinking" duty cycle.

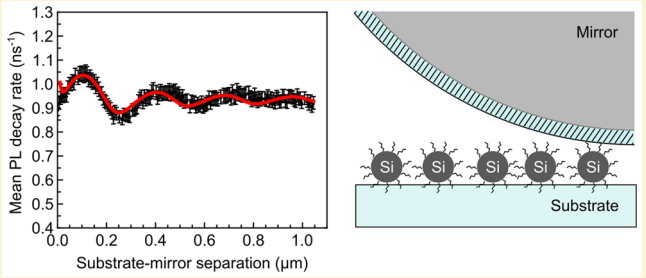

KEYWORDS: *silicon nanoparticles, local density of optical states, photoluminescence, decay rate, quantum efficiency, transition dipole moment*

Silicon has become the cornerstone of CMOS technologies, implemented in microelectronics, photovoltaics, and photodetector technologies. Unfortunately, as an active emitter in lighting or photonic applications silicon is hindered by its indirect band gap. The indirect band gap is characterized by inefficient band-edge absorption and low radiative rates, which result in impractically low photon fluxes and emission efficiencies in the presence of nonradiative channels. The limitations of the indirect band gap can be overcome with silicon nanoparticles (Si-NPs).[1−3] Si-NPs show room-temperature size-tunable luminescence and have many advantageous properties: Si-NPs are photochemically robust and stable due to covalent bonding of ligands,[4,5] they offer spectrally broad photoluminescence (PL), tunable from the near-infrared (IR) to the ultraviolet (UV),[2,3,6] and they are nontoxic (biocompatible and biodegradable[7,8]) and can be biofunctionalized by a large diversity of covalently bonded ligands.[9,10] Since their discovery,[1] the emission efficiency of Si-NPs emitting in the near-IR spectral region has been significantly improved, with reports of external quantum efficiencies (EQEs) exceeding 60%[11,12] (EQE is for an ensemble of emitters given by the ratio of the total number of emitted and absorbed photons). The EQE could see even further improvement, as the internal quantum efficiency (IQE), i.e., the emission quantum efficiency of the subset of the ensemble of emitters that is emissive, has been reported to reach unity.[13−15] The high IQE, which is given by the internal competition between radiative and nonradiative processes, shows that bright subsets within the ensemble of NPs exist for which nonradiative channels are already completely suppressed.

For emission in the visible spectral region below ∼600 nm, the situation is very different. EQEs of intrinsic PL are only sparsely reported on and have not exceeded 20%,[3] which is typically argued to be the consequence of the increased number of surface defects with smaller Si-NPs.[3,16,17] Furthermore, tunability of the PL by the size of the Si-NP through the visible spectral range seems inaccessible for Si-NPs in the presence of oxygen defect states,[18] rendering the most commonly studied

Received: December 31, 2017
Published: April 10, 2018

DOI: 10.1021/acsphotonics.7b01624
ACS Photonics 2018, 5, 2129−2136

oxide-passivated Si-NPs (O:Si-NPs) unsuitable for, e.g., lighting applications.

These limitations can be overcome with a class of Si-NPs capped with organic molecules (C:Si-NPs), which extend emission into the visible spectral region.[2,3,19−22] Moreover, the emission rates in C:Si-NPs have been shown to approach those of direct-bandgap materials,[19−24] suggesting significant enhancement of the radiative recombination rates by 2−3 orders of magnitude compared to hydrogen- or oxide-passivated Si-NPs.[3,19,22−25] These enhanced radiative rates are typically interpreted in terms of the formation of direct-bandgap-like optical transitions due to the electronegative environment[24] or tensile strain induced by the organic ligands,[23] or are related to extrinsic emission sites.[26−28] Nevertheless, despite the greatly enhanced radiative rates in C:Si-NPs, the EQE remains comparatively low in the visible range (<20%).[3,20,22] Possible reasons include the increased number of defects in these small Si-NPs due to disorder, strain and specifically a low surface coverage by organic ligands, as a consequence of steric hindrance. A key question for the application of Si-NPs throughout the visible range is therefore whether the EQE is fundamentally limited to low values or whether in fact subsets of the ensemble of C:Si-NPs do have high intrinsic quantum efficiencies. However, until now, the radiative recombination rate and IQE for Si-NPs emitting in the visible spectral range have been studied only theoretically,[19,23,24] and little is known about the factors that limit the EQE, e.g., efficient nonradiative channels or nonemissive NPs in the ensemble.[29,30]

In this study we investigate the IQE of butyl-passivated Si-NPs (bu:Si-NPs), whose emission is smoothly tunable between 350 and 650 nm via the excitation wavelength. The IQE is measured through modification of the local density of optical states (LDOS) in a Drexhage-type experiment. By this measurement, we experimentally confirm the predicted high radiative rates of C:Si-NPs[19,23,24] and show that this material has an IQE competitive with that of commercially applied dyes and quantum dot phosphors, clearly demonstrating the potential of Si-NPs for lighting applications also for the visible spectral range.

RESULTS AND DISCUSSION

Si-NPs with butyl surface passivation emit in the visible range (Figure 1a,b) and are synthesized using a wet-chemical method, described in detail elsewhere.[10] In short, Si-NPs are obtained by reacting magnesium silicide with bromine in refluxing *n*-octane and are subsequently passivated using *n*-butyllithium.[10] The synthesis yields bu:Si-NPs with a core size of 2.2 ± 0.5 nm, as determined from transmission electron microscopy (TEM, Figure S1).[19,20] The presence of butyl on the surface of the Si-NPs is supported by Fourier-transform infrared (FTIR) spectroscopy (Figure S3), which shows the presence of Si−C (~1260 cm^{-1}) and C−H (~2900 cm^{-1}) stretching modes. In addition, we observe features indicative of oxidation (1000−1100 cm^{-1}), but do not observe the characteristic red emission found in oxidized Si-NPs,[27] suggesting that oxygen has only a minor effect on the emission of bu:Si-NPs. PL dynamics show a high PL recombination rate of ~10^8 s^{-1}, as observed previously,[20] with the PL intensity decaying with an average time of ~3 ns (Figure 1c). The PL decay can be well described by a biexponential, as has been done previously,[20] but can also be fitted well with a stretched-exponential function (for more details see the SI, Figure S4). This applies for bu:Si-NPs dried on a substrate or dispersed in ethanol, as well as for a single bu:Si-NP (inset Figure 1c). Furthermore, in agreement with results in the literature on similar materials, the EQE is very low and is below 6% (Figure S5).[20]

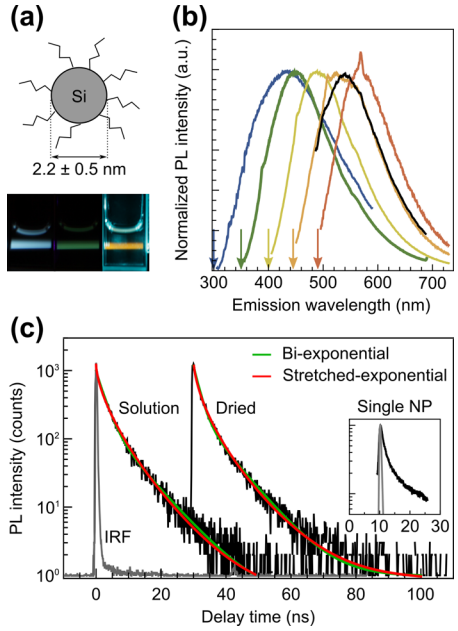

Figure 1. (a) Schematic of the structure of bu:Si-NPs (top) and real-color photos of the PL of bu:Si-NPs in ethanol under 350, 400, and 460 nm pulsed excitation (bottom). (b) PL spectra of bu:Si-NPs in ethanol for different excitation wavelengths, indicated by the arrows. The sharp peak on top of the spectrum excited by 490 nm likely results from Raman-scattered excitation light. The black line shows the PL spectrum of a drop-casted film of bu:Si-NPs under 445 nm excitation. (c) Time-resolved PL of bu:Si-NPs dispersed in ethanol and dried on a substrate under ~450 nm pulsed laser excitation. The curves are shifted along the horizontal axis for presentation purposes and fitted using a biexponential (green) and stretched-exponential (red) function (fit residuals are shown in Figure S4). The gray curve shows the internal response function (IRF) of the detection system used for the dispersion. The IRF for the dried sample measurement has a similar temporal width. Inset: Normalized PL decay of an individual bu:Si-NP (~3.5 kcounts at peak).

To determine the radiative rate and IQE of bu:Si-NPs, we measure the change in the PL decay rate in proximity of a reflective interface using a Drexhage-type setup.[31−36] In particular, we adopt the implementation described by Lunnemann et al.,[37] where a spherical mirror is placed on top of the sample (Figure 2). For this, a thin layer of bu:Si-NPs is drop-casted onto a cleaned quartz substrate from a dispersion of bu:Si-NPs in ethanol. We confirm that the PL spectra and dynamics of the dried thin layer and dispersion are very similar (Figure 1), indicating that the emissive processes are not considerably influenced by both environments.

The IQE is given by the competition between the radiative (γ_r) and nonradiative (γ_{nr}) decay rates: $IQE = \frac{\gamma_r}{\gamma_r + \gamma_{nr}}$. The IQE is extracted from the total PL decay rate $\gamma_{PL} = \gamma_r + \gamma_{nr}$ by controllably varying the radiative rate γ_r through controlled variation of the LDOS near the mirror surface,[38] ρ: $\gamma_r = \gamma_r^{vac}\frac{\rho}{\rho^{vac}}$. The mirror affects the LDOS, but does not modify the direct environment of the emitter, so that the intrinsic nonradiative decay rate is not influenced. We use a spherical lens coated with an optically thick layer of silver[37] placed on top of the sample (Figure 2a). Using an inverted scanning confocal microscope

DOI: 10.1021/acsphotonics.7b01624
ACS Photonics 2018, 5, 2129−2136

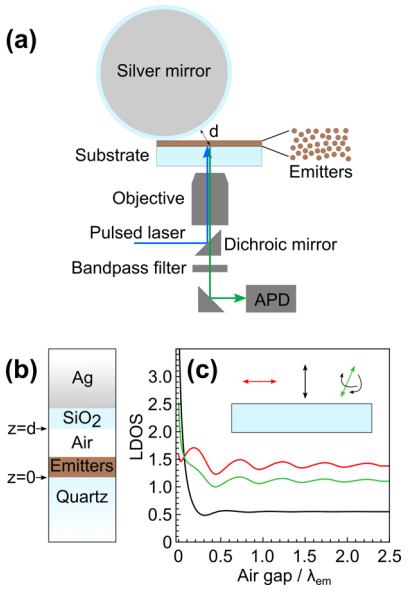

Figure 2. (a) Schematic of the experimental setup. (b) Sketch of the stratified medium specific to our experimental setup that is assumed for LDOS calculations. (c) LDOS calculated for our geometry for emitters with the dipole oriented parallel (red) and perpendicular (black) to the interface, against the air gap normalized to the emission wavelength. Green curve shows the isotropic LDOS. The parameters used for the LDOS calculations are shown in Table S1.

we then excite PL from the NP layer with a 455 or 480 nm wavelength ps-pulsed laser and detect the arrival times of the emitted photons using an avalanche photodiode (APD). By scanning the area around the point where the silver-coated lens touches the sample, different emitter−mirror separations, d, are probed. The large radius of curvature of the lens (2 mm) ensures that the emitters effectively experience an almost flat mirror and that a large in-plane scan range of ∼60 μm gives exquisite resolution over the separation d, which spans a range of ∼1 μm. Thereby the LDOS, $\rho(d)$, is controllably varied in the presented setup. To be able to extract the IQE, the LDOS is calculated using Amos and Barnes' implementation[35] of the methodology introduced by Chance, Prock, and Silbey,[39] where we can account for all the different layers in our sample stack, at least on the assumption that the emitter is located inside a stack of parallel layers (Figure 2b). The LDOS calculated for the two principal dipole orientations is shown in Figure 2c, corresponding to the two static orientations of the emission transitions dipole moment (TDM), oriented parallel or perpendicular to the substrate. Also the isotropic LDOS is shown, which describes the LDOS experienced by an individual dipole that rotates quickly compared to the PL lifetime ($\theta < \tau_{PL}$),[40] but also describes the mean LDOS of an ensemble of randomly oriented static dipoles. In both cases, all directions are sampled and the LDOS is given by a 2/3 to 1/3 mixture of parallel and perpendicular dipole orientations. Finally, the IQE, η, can be extracted from the dependence of the decay rate on the emitter−mirror separation (d) and the LDOS corresponding to the relevant dipole orientation (ρ):

$$\gamma_{PL}(d) = \gamma_{PL}(\infty)\left\{1 + \eta\left[\frac{\rho(d)}{\rho(\infty)} - 1\right]\right\} \quad (1)$$

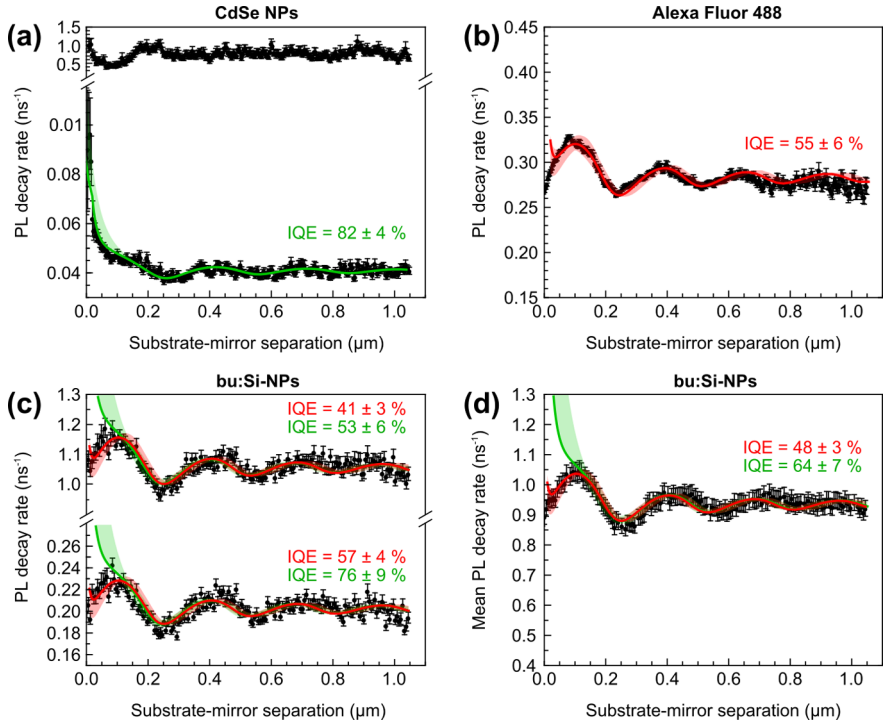

Figure 3. (a) PL decay rate as a function of the substrate−mirror separation for CdSe NPs, (b) Alexa 488 Fluor, and (c, d) bu:Si-NPs under 480, 480, and 455 nm excitation wavelengths, respectively. The two curves shown for (a) the CdSe NPs and (c) the bu:Si-NPs represent both components of the decay rate obtained by fitting the PL decay dynamics to a biexponential decay. For the bu:Si-NPs, also the mean decay rate obtained by fitting the PL decay with a stretched-exponential function is shown in panel d. Green lines represent fits assuming the mean isotropic LDOS, whereas red lines represent fits assuming the mean parallel LDOS. Shaded areas show the uncertainty in the fits resulting from uncertainties in the refractive indices and dimensions of the system and from the width of the detected emission wavelengths (see Table S2).

DOI: 10.1021/acsphotonics.7b01624
ACS Photonics 2018, 5, 2129−2136

where $\gamma_{PL}(\infty)$ and $\rho(\infty)$ are the decay rate and LDOS in the absence of the mirror.

To verify the setup, in addition to the bu:Si-NPs we measure two commercially available reference materials, CdSe-based NPs and Alexa 488 fluorophores, both drop-casted from a solution onto a cleaned quartz substrate (Figures S6 and S7). We use a maximum entropy method (MEM)[41] to analyze the decay dynamics, showing that the PL decay of the CdSe NPs is best described by a biexponential function (Figure S6). We use the biexponential model to extract the two components of the decay rate as a function of the distance from the mirror (Figure 3a). For the slower component (bottom), we obtain clear oscillations in the PL decay rate. Fourier analysis shows that the period of the oscillations is correlated with the period of the LDOS (Figure S9), confirming that the radiative component is modified by the varied LDOS in proximity of the mirror. At distances below $d \approx 100$ nm we observe a strong decay rate enhancement, indicating the coupling of the emitters to surface plasmon polariton modes. This is characteristic for an isotropic dipole orientation (Figure 2c). The strong dependence of the decay rate on the LDOS is indicative of a significant radiative contribution to the PL decay rate, which is expected for high-efficiency fluorophores. The fast decay component (top) shows no clear dependence on the emitter−mirror separation, indicating that it is mainly of nonradiative character.

For the Alexa Fluor, the PL decay is well described by a monoexponential function (Figure S7). Similarly to the CdSe NPs, the decay rate shows clear oscillations with the distance from the mirror, with a frequency correlated to that of the oscillation frequency of the LDOS (Figure S9). However, in contrast to the CdSe NPs, the drop-casted layer of the Alexa dye shows no decay rate enhancement at close proximity to the mirror, characteristic for a static dipole orientation that is parallel with respect to the substrate (Figure 2c). Again the high amplitude of the observed oscillations indicates a strong radiative character of the PL decay rate.

The PL decay rate of bu:Si-NPs is shown in Figure 3c and d, obtained by fitting the PL decay with a biexponential function and with a stretched-exponential function, both which result in satisfactory fit residuals (Figure S4). The decay models convey a different physical mechanism underlying the PL. The biexponential decay suggests the overlapping signal from two subpopulations of NPs in the sample, whereas the stretched-exponential decay is characteristic for a single population that is broadened, e.g., due to an intrinsic size distribution or variation in the local environment. We find that for both models the decay rate components show well-defined oscillations with a high amplitude (Figure 3c,d). Interestingly, when assuming biexponential decay dynamics, the high amplitude of the oscillations shows that both components have a strongly radiative character. This is unexpected, as the faster decay component could be anticipated to result from a strong nonradiative decay, as observed for the CdSe NPs, where the fast decay rate component is unaffected by the proximity to the mirror (top of Figure 3a). This surprising result for bu:Si-NPs could suggest that the two observed PL decay components, also observed in dispersion and for a single bu:Si-NP (Figure 1c), correspond to two separate emissive states of a bu:Si-NP. However, it is unlikely to have two separate emissive states with such a similar IQE value, rather suggesting that these states are closely related. We therefore expect the physics to be described more accurately by a stretched-exponential model, which is supported by the MEM analysis (Figure S11).

For both models, the decay rates are best fitted to eq 1 for a static parallel dipole orientation (red curve in Figure 3c,d), which yields values for the IQE of ∼41% and ∼57% and radiative rates of 0.44 ± 0.03 ns^{-1} and 0.11 ± 0.01 ns^{-1} for the faster and slower decay components of the biexponential decay, respectively. For the stretched-exponential model we obtain a very similar IQE of ∼48% and a mean radiative rate of 0.45 ± 0.03 ns^{-1}. Assuming an isotropic dipole orientation instead (green curve in Figure 3), typically expected for semiconductor nanoparticles with a band-like energy dispersion, yields higher values for the IQEs of ∼53% and ∼76% with radiative rates of 0.49 ± 0.05 ns^{-1} and 0.13 ± 0.02 ns^{-1} for the biexponential model and ∼64% with a radiative rate of 0.60 ± 0.06 ns^{-1} for the stretched-exponential model, but provides a poorer fit at short distances ($d < 100$ nm). We conclude that the already very high IQE values fitted by the parallel dipole orientation case are in fact conservative estimates of the IQE.

To better understand the LDOS character of the decay rate modifications of the bu:Si-NPs, we first analyze the difference in the LDOS character observed for the CdSe NP and the Alexa Fluor reference materials (Figure 3). These differences can be explained in terms of the orientation of the emission TDM of both emitters (Figure 2c). The experimentally determined average decay rate depends not only on the decay rate of each individual emitter but also on the number of photons that each orientation contributes to the total PL signal.[42,43] As a result, the decay rate of the total PL intensity will be determined mainly by the emitters with TDM orientations that are efficiently excited and that couple well to modes that radiate into the far-field detector (i.e., that are not quenched). Since the distribution of decay rates is narrow in an ensemble of emitters with a quickly rotating emission TDM such as in CdSe NPs,[44] the average decay rate is well described by the isotropic LDOS,[32,37] as observed in our measurement in Figure 3a. In contrast, for emitters with a static emission TDM, the decay rate and emission brightness are strongly orientation-dependent (Figure 2c). In this case, the average decay rate of the ensemble is determined by the dipole orientations that are most efficiently excited and that most efficiently radiate toward the detection system, which in our setup is expected to concern dipoles that are oriented parallel to the substrate.[42] The quantitative ramifications of this orientation selectivity depend on the specific details of the setup, i.e., the numerical aperture (NA) of the excitation and detection system,[42] and on the orientation of the emitter's absorption and emission TDM. Indeed, the Alexa 488 Fluor is expected to have a TDM that is locked to its molecular structure and well aligned with the absorption dipole moment. Given that the molecule is structurally flat, drop-casting might lead to preferential arrangement of dipoles parallel to the substrate, which further strengthens the mainly parallel LDOS contribution to the PL decay in Figure 3b.

To confirm the orientation of the TDM, we carried out PL polarization anisotropy measurements (Figure 4). The PL anisotropy, a, is determined from the difference between the intensity of the detected PL intensity with a polarization parallel ($I_{\parallel}$) and perpendicular ($I_{\perp}$) to the excitation polarization direction: $a(t) = \frac{I_{\parallel}(t) - I_{\perp}(t)}{I_{\parallel}(t) + 2I_{\perp}(t)}$. The decay of the PL anisotropy over time defines the intrinsic depolarization time (θ_{pol}) of the studied emitters. For the CdSe NPs we observe no PL anisotropy (Figure 4a), suggesting depolarization faster than the time resolution of our system, which is expected for a

DOI: 10.1021/acsphotonics.7b01624
ACS Photonics 2018, 5, 2129−2136

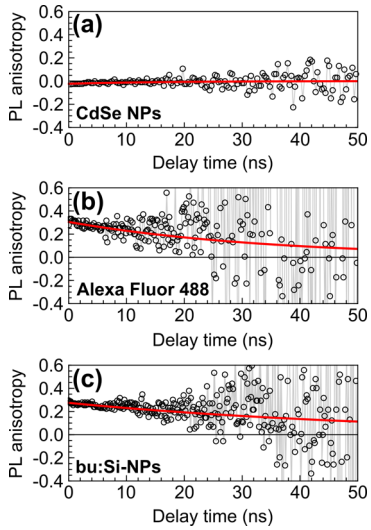

Figure 4. Time-resolved PL anisotropy, after excitation with a linearly polarized pulsed laser (488 nm) of emitters dried on a substrate. Red solid lines show monoexponential fits. While we do not observe PL anisotropy for the CdSe NPs (a), we find an initial anisotropy of 0.35 for the Alexa 488 Fluor (b), which is in excellent agreement with values found in the literature (see, for example, ref 45). For bu:Si-NPs (c) we find an initial anisotropy of ∼0.3, which decays within 10's of ns.

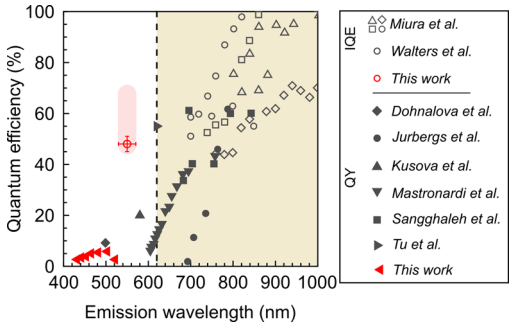

Figure 5. Overview of the IQE (open symbols) and EQE (filled symbols) of bu:Si-NPs (red symbols) obtained in this work compared to values found in the literature for different types of Si-NPs (gray symbols). The yellow-shaded area indicates the spectral region for which high QY and IQE values have been reported in the literature. IQEs are from Miura et al.[13] and Walters et al.,[48] and EQEs are from Dohnalova et al.,[19] Jurbergs et al.,[11] Kusova et al.,[22] Mastronardi et al.,[17] Sangghaleh et al.,[14] and Tu et al.[53] The IQE obtained for bu:Si-NPs assumes a parallel dipole orientation and stretched-exponential decay dynamics. The shaded areas above indicate the range of IQE obtained for an isotropic dipole orientation.

degenerate TDM.[44] For the Alexa Fluor we find an initial anisotropy of ∼0.35, which decays only slowly within tens of ns, confirming the static TDM[45] ($\theta_{po} < \tau_{PL}$). The difference in the emission TDM character between the CdSe NPs and Alexa Fluor is in good agreement with the difference in LDOS character observed in Figure 3a,b.

Interestingly, the PL anisotropy measured for the bu:Si-NPs shows a static emission TDM similar to that of the Alexa Fluor (Figure 4c), with an initial PL anisotropy of ∼0.3 that decays within ∼50 ns. In analogy with the CdSe NPs, we would rather expect an isotropic fast rotating dipole orientation for the bu:Si-NPs due to the assumed band-to-band TDM that is typically degenerate.[46] The static nature of the TDM of bu:Si-NPs could suggest that emission is governed by localized states[46] around the band gap, most likely contributed by the covalently bonded organic ligands.[19,23,24] Alternatively this could be due to a slightly anisotropic shape of the Si-NPs.[47] In any case, similarly to the Alexa Fluor, the static TDM results in a detection bias toward parallel dipole orientations also for the bu:Si-NPs,[42] although the detection of a purely parallel LDOS is not justified due to the high NA objective (NA = 1.45) used for these experiments.[42]

Independent of the precise physics underlying the TDM orientation, it is evident that, according to our data, the most conservative estimates of the IQE are ∼48% with an associated mean radiative rate of ∼0.45 ns^{-1} for the stretched-exponential model. This radiative rate, determined here for the first time, is in good agreement with our theoretically predicted rates for C:Si-NPs.[19,24] Another important finding is that this lower limit of the IQE is high in comparison with the EQEs measured by us and encountered in the literature, for intrinsic PL of Si-NPs emitting below ∼620 nm, as shown in Figure 5. This thus demonstrates that bu:Si-NPs can emit very efficiently, provided that they are optically active. The fact that the ensemble EQE is much lower (below ∼6%) indicates the existence of a large fraction of nonemissive ("dark") NPs that dilute the efficiency of the ensemble, by contributing to absorption but not to emission. Indeed the presence of nonemissive NPs is commonly invoked to explain the discrepancy between the EQE and IQE of Si-NPs in literature,[48] where the dark fraction is anticipated to be either due to permanently dark NPs[29,49] or due to temporarily dark NPs, as a consequence of PL "blinking".[50] To find the responsible cause of the low emissive fraction of bu:Si-NPs, we carried out PL measurements on individual NPs (Figure S12). These measurements reveal that bu:Si-NPs are most of the time switched OFF, suggesting that PL blinking is for the majority responsible for the low ensemble EQE. Hence there is a possibility to improve the EQE to (at least) the level of the IQE of ∼48% measured here, if a way can be found to resolve the mechanisms that cause PL blinking in this type of Si-NPs. For this, the quality of the surface passivation is likely to play a crucial role.[51,52]

CONCLUSION

In conclusion, we report for the first time the experimentally determined IQE and radiative rates of Si-NPs emitting in the visible range (<620 nm) by means of a Drexhage-type experiment. In good agreement with our previous theoretical studies,[19,24] we find a high mean radiative rate of ∼0.45 ns^{-1}, comparable to the radiative rates of direct-bandgap materials and fluorescent dyes. Moreover, the IQE of roughly 48% determined here for emission at ∼550 nm is, to the best of our knowledge, the highest reported value for intrinsic PL of Si-NPs in this spectral range. Comparison with single-NP measurements demonstrates that the major limitation of the emission efficiency of Si-NPs is the presence of nonemissive (dark) NPs in the ensemble, most likely due to a low blinking duty cycle. The high IQE shows the potential of organically capped Si-NPs for lighting and bioimaging applications, where they possibly can replace toxic, expensive, and or rare phosphors, such as CdSe- or In-based NPs. An excellent question for future research is what mechanisms precisely cause bu:Si-NPs to be dark and how to counteract those mechanisms.

DOI: 10.1021/acsphotonics.7b01624
ACS Photonics 2018, 5, 2129−2136

MATERIALS AND METHODS

Materials. CdSe/ZnSe/ZnS (core/shell/shell) NPs emitting around 590 nm (CANdots Series A CSS) in hexane were purchased from the Center for Applied Nanotechnology (CAN) GmbH. Alexa 488 (Alexa Fluor 488) was purchased from Thermo Fisher Scientific and was dissolved in UV-grade ethanol.

NPs in Solution. Bu:Si-NPs dispersed in UV-grade ethanol are measured inside quartz cuvettes (Hellma Analytics). PL spectra are recorded using a spectrofluorometer (Horiba Scientific, Fluorolog) equipped with a spectrometer (Horiba Scientific, iHR320) and a CCD camera (Horiba Scientific, Synapse). PL spectra are corrected for the spectral sensitivity of the system. Time-resolved PL was measured using a PMT (Hamamatsu R3809U-51) using a bin time of 0.1 ns, with excitation provided by a 445 nm wavelength diode laser (Lasos, BDL-SMN series), operated at 10 MHz with a ∼40 ps pulse width.

Single-NP PL. PL of individual bu:Si-NPs was measured using an inverted confocal microscope system (Picoquant, MicroTime 200) equipped with a 60× water immersion objective (Olympus). The excitation was provided by a 405 nm ps-pulsed laser diode (Picoquant, LDH-D-C-400B) operated at 40 MHz. Emission was detected using an APD (PerkinElmer, SPCM AQR-14).[20]

Dried NP Layers. Quartz coverslips (Structure Probe Inc.) were cleaned in an alkaline cleaning solution (base-piranha or Hellmanex III) followed by a UV dry-cleaning procedure (oxygen descum or ozone treatment). The samples were prepared by drop-casting a dispersion containing the emitters on the cleaned substrate. PL spectra were acquired using an inverted microscope (Zeiss, Axio observer Z1) coupled to a spectrometer (Princeton Instruments, Acton SP2300) equipped with a CCD camera (Princeton Instruments, Pylon400B).

Time-Resolved PL Imaging. The dried NP samples are studied using an inverted confocal microscope, where the NPs are excited by a pulsed laser that is focused to a diffraction-limited spot with a high NA immersion microscope objective. Emitted photons are collected with the same objective, filtered through a band-pass filter, and detected using an APD. For the silicon-based samples we used a supercontinuum laser (Fianium) operating at 10 MHz (∼3 μW) filtered by an acousto-optical tunable filter (450−460 nm), a Nikon Eclipse Ti-U inverted microscope equipped with a 100× oil immersion objective lens (Nikon, Plan Apo Lambda, NA = 1.45), and an APD from ID-Quantique (ID100-20) connected to a Becker and Hickl DPC230 correlator card (0.16 ns per bin). The emission was filtered through a 550 ± 20 nm band-pass filter. For the CdSe NPs and Alexa dye we used an Olympus FV1000 microscope and a 60× water immersion objective lens (Olympus, UPLS Apo, NA = 1.2). PL was excited by a 480 nm laser diode (Picoquant, LDH-P-C-485) operated at 5 MHz (∼10 μW) or 20 MHz (∼4 μW). The emission for the CdSe NPs and Alexa dye was filtered by a 593 ± 20 nm and 537 ± 13 nm band-pass filter, respectively, and detected using an APD (MPD, PDM) connected to a time-correlated single-photon counting module (Picoquant, Picoharp). Data were binned in time bins of 0.512 and 0.16 ns. The LDOS is controlled by placing a silver-coated spherical lens on top of the sample. When scanning the sample at different positions, different separations between the mirror and the substrate are probed, which effectively leads to modification of the LDOS. The distance to the mirror at any position, $\mathbf{r}$, on the sample is calculated from the distance to the contact point of the mirror with the sample, $\mathbf{r_0}$, and the diameter of the mirror, R: $x = \sqrt{(|\mathbf{r} - \mathbf{r_0}|^2 + R^2} - R$. PL decays are then constructed from a histogram of the photon arrival times recorded at positions on the sample that lie within concentric rings with contact points of the sphere with the sample (see Figure S7).

Mirror Preparation. The mirrors were prepared from spherical lenses (Edmund Optics, S-LAH79) with a diameter of 4 or 6 mm, which were cleaned in a base-piranha solution and glued to coverslips. Using electron beam physical vapor deposition the spheres were coated with 5 nm of germanium, 100 nm of silver, and finally 35 nm of SiO_2.

LDOS Calculations. For LDOS calculations we used Amos and Barnes'[35] implementation of the method introduced by Chance et al.[39] The geometries found in Urbach and Rikken[54] and Novotny and Hecht[55] were used to verify our calculated LDOS values for geometries involving dielectrics and metals, respectively. The used LDOS is taken to be the average LDOS within the detection volume.

Data Analysis. PL decay rates, $\gamma_{PL}(d)$, are extracted by fitting a mono- or biexponential function to the falling edge of the PL decay by optimization of the log-likelihood, assuming that the data follow a Poissonian probability distribution due to photon-counting noise. To extract the IQE, the decay rates are then fitted by eq 1. For calculation of the substrate-mirror separation we accounted for the thickness of the emitter layer and corrected for the shift resulting from potential damage to the mirror (for a detailed discussion refer to the SI). The uncertainty of the obtained IQE and radiative decay rate values result from uncertainties in LDOS arising from the uncertainty in the refractive indices and dimensions of the system and from the width of the detected emission band (see Table S2).

PL Anisotropy. For anisotropy measurements, PL is excited in a right-angle geometry by the linearly polarized light from a 488 nm diode laser (Lasos, BDL-SMN series) filtered through a linear polarizer. Emitted photons are collected by a NA = 0.1 lens and filtered first by a 550-40 bandpass filter and then by a linear polarization filter oriented parallel or perpendicular to the polarization of the excitation light. Finally, the emission is detected using an APD (ID Quantique, ID100-50). The arrival times of the detected photons with respect to the pump pulse are recorded with a timing card (Becker & Hickl, DPC-230). The measurements were corrected for the detection efficiency of both polarization directions, by exciting the sample with horizontally polarized light.

ASSOCIATED CONTENT

Supporting Information

The Supporting Information is available free of charge on the ACS Publications website at DOI: 10.1021/acsphotonics.7b01624.

More details on the sample characterization, PL decay analysis, Fourier analysis, and LDOS calculations (PDF)

AUTHOR INFORMATION

Corresponding Author

*E-mail: k.newell@uva.nl.

ORCID

Bart van Dam: 0000-0001-8880-9389

A. Femius Koenderink: 0000-0003-1617-5748

DOI: 10.1021/acsphotonics.7b01624
ACS Photonics 2018, 5, 2129−2136

Author Contributions

The manuscript was written through contributions of all authors. All authors have given approval to the final version of the manuscript. B.v.D., R.M., and C.I.O. performed the Drexhage-type experiments; B.v.D. carried out the data analysis and PL anisotropy measurements; M.A.H. facilitated and helped with the time-resolved PL and anisotropy measurements; A.F.K. provided the scripts for LDOS calculations; A.F.K. and K.D. conceived and supervised the project.

Notes

The authors declare no competing financial interest.

[⊥]K.D. is presently Katerina Newell.

■ ACKNOWLEDGMENTS

B.v.D. and K.D. acknowledge Dutch STW funding (No. 12146), FOM Projectruimte (No. 15PR3230), and a MacGillavry Fellowship. This work was supported by The Netherlands Organization for Scientific Research (NWO): M.A.H. acknowledges support via a NWO "Middelgroot" investment grant (834.09.003); A.F.K. gratefully acknowledges a NWO-Vidi and Vici grant for financial support; C.I.O. acknowledges support by an industrial partnership program between Philips Lighting and NWO. The authors would like to thank Prof. T. Gregorkiewicz (University of Amsterdam) for facilitating this project. Moreover, the authors are grateful to A. Lof (AMOLF) for preparation of the mirrors, C. Umesh, J. Paulusse and H. Zuilhof (Wageningen University) for the sample preparation, A. Poddubny (Ioffe Institute) for fruitful discussions, and M. Postma (University of Amsterdam) for his help with the MEM analysis.

■ REFERENCES

(1) Canham, L. T. Direct Observation of Individual Nanometer-Sized Light-Emitting Structures on Porous Silicon Surfaces. *Appl. Phys. Lett.* **1990**, *57*, 1046−1048.

(2) Shirahata, N. Colloidal Si Nanocrystals: A Controlled Organic − Inorganic Interface and Its Implications of Color-Tuning and Chemical Design toward Sophisticated Architectures. *Phys. Chem. Chem. Phys.* **2011**, *13*, 7284−7294.

(3) Dohnalova, K.; Gregorkiewicz, T.; Kusova, K. Silicon Quantum Dots: Surface Matters. *J. Phys.: Condens. Matter* **2014**, *26*, 173201.

(4) Warner, J. H.; Hoshino, A.; Yamamoto, K.; Tilley, R. D. Water-Soluble Photoluminescent Silicon Quantum Dots. *Angew. Chem.* **2005**, *117*, 4626−4630.

(5) He, Y.; Zhong, Y.; Peng, F.; Wei, X.; Su, Y.; Lu, Y.; Su, S.; Gu, W.; Liao, L.; Lee, S.-T. One-Pot Microwave Synthesis of Water-Dispersible, Ultraphoto- and pH-Stable, and Highly Fluorescent Silicon Quantum Dots. *J. Am. Chem. Soc.* **2011**, *133*, 14192−14195.

(6) Kang, B. Z.; Liu, Y.; Tsang, C. H. A.; Duo, D.; Ma, D.; Fan, X.; Wong, N.-B.; Lee, S.-T. Water-Soluble Silicon Quantum Dots with Wavelength-Tunable Photoluminescence. *Adv. Mater.* **2009**, *21*, 661−664.

(7) Liu, J.; Erogbogbo, F.; Yong, K.-T.; Ye, L.; Liu, J.; Hu, R.; Chen, H.; Hu, Y.; Yang, Y.; Yang, J.; et al. Assessing Clinical Prospects of Silicon Quantum Dots: Studies in Mice and Monkeys. *ACS Nano* **2013**, *7*, 7303−7310.

(8) Park, J.-H.; Gu, L.; Maltzahn, G.; Von; Ruoslahti, E.; Bhatia, S. N.; Sailor, M. J. Biodegradable Luminescent Porous Silicon Nanoparticles for in Vivo Applications. *Nat. Mater.* **2009**, *8*, 331−336.

(9) Veinot, J. G. C. Synthesis, Surface Functionalization, and Properties of Freestanding Silicon Nanocrystals. *Chem. Commun.* **2006**, *40*, 4160−4168.

(10) Ruizendaal, L.; Pujari, S. P.; Gevaerts, V.; Paulusse, J. M. J.; Zuilhof, H. Biofunctional Silicon Nanoparticles by Means of Thiol-Ene Click Chemistry. *Chem. - Asian J.* **2011**, *6*, 2776−2786.

(11) Jurbergs, D.; Rogojina, E.; Mangolini, L.; Kortshagen, U. Silicon Nanocrystals with Ensemble Quantum Yields Exceeding 60%. *Appl. Phys. Lett.* **2006**, *88*, 60−63.

(12) Mobarok, H.; Purkait, T. K.; Islam, M. A.; Miskolzie, M.; Veinot, J. G. C. Instantaneous Functionalization of Chemically Etched Silicon Nanocrystal Surfaces. Angew. *Angew. Chem.* **2017**, *129*, 6169−6173.

(13) Miura, S.; Nakamura, T.; Fujii, M.; Inui, M.; Hayashi, S. Size Dependence of Photoluminescence Quantum Efficiency of Si Nanocrystals. *Phys. Rev. B: Condens. Matter Mater. Phys.* **2006**, *73*, 245333.

(14) Sangghaleh, F.; Sychugov, I.; Yang, Z.; Veinot, J. G. C.; Linnros, J. Near-Unity Internal Quantum Efficiency of Luminescent Silicon Nanocrystals with Ligand Passivation. *ACS Nano* **2015**, *9*, 7097−7104.

(15) Greben, M.; Khoroshyy, P.; Liu, X.; Pi, X.; Valenta, J. Fully Radiative Relaxation of Silicon Nanocrystals in Colloidal Ensemble Revealed by Advanced Treatment of Decay Kinetics. *J. Appl. Phys.* **2017**, *122*, 34304.

(16) Sun, W.; Qian, C.; Wang, L.; Wei, M.; Mastronardi, M. L.; Casillas, G.; Breu, J.; Ozin, G. A. Switching-on Quantum Size Effects in Silicon Nanocrystals. *Adv. Mater.* **2015**, *27*, 746−749.

(17) Mastronardi, M. L.; Maier-Flaig, F.; Faulkner, D.; Henderson, E. J.; Kubel, C.; Lemmer, U.; Ozin, G. A. Size-Dependent Absolute Quantum Yields for Size-Separated Colloidally-Stable Silicon Nanocrystals. *Nano Lett.* **2012**, *12*, 337−342.

(18) Wolkin, M. V.; Jorne, J.; Fauchet, P. M.; Allan, G.; Delerue, C. Electronic States and Luminescence in Porous Silicon Quantum Dots: The Role of Oxygen. *Phys. Rev. Lett.* **1999**, *82*, 197−200.

(19) Dohnalova, K.; Poddubny, A. N.; Prokofiev, A. A.; de Boer, W. D. A. M.; Umesh, C. P.; Paulusse, J. M. J.; Zuilhof, H.; Gregorkiewicz, T. Surface Brightens up Si Quantum Dots: Direct Bandgap-like Size-Tunable Emission. *Light: Sci. Appl.* **2013**, *2*, e47.

(20) Dohnalova, K.; Fucikova, A.; Umesh, C. P.; Humpolickova, J.; Paulusse, J. M. J.; Valenta, J.; Zuilhof, H.; Hof, M.; Gregorkiewicz, T. Microscopic Origin of the Fast Blue-Green Luminescence of Chemically Synthesized Non-Oxidized Silicon Quantum Dots. *Small* **2012**, *8*, 3185−3191.

(21) English, D. S.; Pell, L. E.; Yu, Z.; Barbara, P. F.; Korgel, B. A. Size Tunable Visible Luminescence from Individual Organic Monolayer Stabilized Silicon Nanocrystal Quantum Dots. *Nano Lett.* **2002**, *2*, 681−685.

(22) Kusová, K.; Cibulka, O.; Dohnalová, K.; Pelant, I.; Valenta, J.; Fucíková, A.; Žídek, K.; Lang, J.; Englich, J.; Matějka, P.; et al. Brightly Luminescent Organically Capped Silicon Nanocrystals Fabricated at Room Temperature and Atmospheric Pressure. *ACS Nano* **2010**, *4*, 4495−4504.

(23) Kusová, K.; Hapala, P.; Valenta, J.; Jelínek, P.; Cibulka, O.; Ondič, L.; Pelant, I. Direct Bandgap Silicon: Tensile-Strained Silicon Nanocrystals. *Adv. Mater. Interfaces* **2014**, *1*, 1−9.

(24) Poddubny, A. N.; Dohnalova, K. Direct Band Gap Silicon Quantum Dots Achieved via Electronegative Capping. *Phys. Rev. B: Condens. Matter Mater. Phys.* **2014**, *90*, 245439.

(25) Guerra, R.; Ossicini, S. High Luminescence in Small Si/SiO_2 Nanocrystals: A Theoretical Study. *Phys. Rev. B: Condens. Matter Mater. Phys.* **2010**, *81*, 245307.

(26) Dasog, M.; Yang, Z.; Regli, S.; Atkins, T. M.; Faramus, A.; Singh, M. P.; Muthuswamy, E.; Kauzlarich, S. M.; Tilley, R. D.; Veinot, J. G. C. Chemical Insight into the Origin of Red and Blue Photoluminescence Arising from Freestanding Silicon Nanocrystals. *ACS Nano***2013**, *7*, 2676−268510.1021/nn4000644.

(27) Sinelnikov, R.; Dasog, M.; Beamish, J.; Meldrum, A.; Veinot, J. G. C. Revisiting an Ongoing Debate: What Role Do Surface Groups Play in Silicon Nanocrystal Photoluminescence? *ACS Photonics* **2017**, *4*, 1920−1929.

(28) Dasog, M.; De Los Reyes, G. B.; Titova, L. V.; Hegmann, F. A.; Veinot, J. G. C. Size vs Surface: Tuning the Photoluminescence of Freestanding Silicon Nanocrystals Across the Visible Spectrum via Surface Groups. *ACS Nano* **2014**, *8*, 9636−9648.

DOI: 10.1021/acsphotonics.7b01624
ACS Photonics 2018, 5, 2129−2136

(29) Credo, G. M.; Mason, M. D.; Buratto, S. K. External Quantum Efficiency of Single Porous Silicon Nanoparticles. *Appl. Phys. Lett.* **1999**, *74*, 1978−1980.
(30) Limpens, R.; Gregorkiewicz, T. Spectroscopic Investigations of Dark Si Nanocrystals in SiO_2 and Their Role in External Quantum Efficiency Quenching. *J. Appl. Phys.* **2013**, *114*, 74304.
(31) Drexhage, K.; Fleck, M.; Schafer, F.; Sperling, W. Beeinflussing Der Fluoreszenz Eines Europium-Chelates Durch Einen Spiegel. *Ber. Bunsen. Phys. Chem.* **1966**, *20*, 1179.
(32) Leistikow, M. D.; Johansen, J.; Kettelarij, A. J.; Lodahl, P.; Vos, W. L. Size-Dependent Oscillator Strength and Quantum Efficiency of CdSe Quantum Dots Controlled via the Local Density of States. *Phys. Rev. B: Condens. Matter Mater. Phys.* **2009**, *79*, 45301.
(33) Buchler, B. C.; Kalkbrenner, T.; Hettich, C.; Sandoghdar, V. Measuring the Quantum Efficiency of the Optical Emission of Single Radiating Dipoles Using a Scanning Mirror. *Phys. Rev. Lett.* **2005**, *95*, 63003.
(34) Snoeks, E.; Lagendijk, A.; Polman, A. Measuring and Modifying the Spontaneous Emission Rate of Erbium near an Interface. *Phys. Rev. Lett.* **1995**, *74*, 2459−2462.
(35) Amos, R. M.; Barnes, W. L. Modification of the Spontaneous Emission Rate of Eu^{3+} Ions close to a Thin Metal Mirror. *Phys. Rev. B: Condens. Matter Mater. Phys.* **1977**, *55*, 7249−7254.
(36) Chizhik, A. I.; Chizhik, A. M.; Khoptyar, D.; Sebastian, B.; Meixner, A. J.; Enderlein, J. Probing the Radiative Transition of Single Molecules with a Tunable Microresonator. *Nano Lett.* **2011**, *11*, 1700−1703.
(37) Lunnemann, P.; Rabouw, F. T.; van Dijk-Moes, R. J. A.; Pietra, F.; Vanmaekelbergh, D.; Koenderink, A. F. Calibrating and Controlling the Quantum Efficiency Distribution of Inhomogeneously Broadened Quantum Rods by Using a Mirror Ball. *ACS Nano* **2013**, *7*, 5984−5992.
(38) Sprik, R.; van Tiggelen, B. A.; Lagendijk, A. Optical Emission in Periodic Dielectrics. *Europhys. Lett.* **1996**, *35*, 265−270.
(39) Chance, R. R.; Prock, A.; Silbey, R. Molecular Fluorescence and Energy Transfer near Interfaces. *Adv. Chem. Phys.* **2007**, *37*, 1−65.
(40) Barnes, W. L. Fluorescence near Interfaces: The Role of Photonic Mode Density. *J. Mod. Opt.* **1998**, *45*, 661−699.
(41) Brochon, J.-C. Maximum Entropy Method of Data Analysis in Time-Resolved Spectroscopy. In *Methods in Enzymology*; Academic Press, 1994; Vol. *240*, pp 262−311.
(42) Danz, N.; Heber, J.; Brauer, A.; Kowarschik, R. Fluorescence Lifetimes of Molecular Dye Ensembles near Interfaces. *Phys. Rev. A: At., Mol., Opt. Phys.* **2002**, *66*, 63809.
(43) Koenderink, A. F.; Kafesaki, M.; Soukoulis, C. M.; Sandoghdar, V. Spontaneous Emission Rates of Dipoles in Photonic Crystal Membranes. *J. Opt. Soc. Am. B* **2006**, *23*, 1196−1206.
(44) Empedocles, S. A.; Neuhauser, R.; Bawendi, M. G. Three-Dimensional Orientation Measurements of Symmetric Single Chromophores Using Polarization Microscopy. *Nature* **1999**, *399*, 126−130.
(45) Rusinova, E.; Tretyachenko-Ladokhina, V.; Vele, O. E.; Senear, D. F.; Ross, J. B. A. Alexa and Oregon Green Dyes as Fluorescence Anisotropy Probes for Measuring Protein − Protein and Protein − Nucleic Acid Interactions. *Anal. Biochem.* **2002**, *308*, 18−25.
(46) Schmidt, T.; Chizhik, A. I.; Chizhik, A. M.; Potrick, K.; Meixner, A. J.; Huisken, F. Radiative Exciton Recombination and Defect Luminescence Observed in Single Silicon Nanocrystals. *Phys. Rev. B: Condens. Matter Mater. Phys.* **2012**, *86*, 125302.
(47) Andrianov, A. V.; Kovalev, D. I.; Zinov'ev, N. N.; Yaroshetskii, I. D. Anomalous Photoluminescence Polarization of Porous Silicon. *Am. Inst. Phys.* **1993**, *58*, 427−430.
(48) Walters, R. J.; Kalkman, J.; Polman, A.; Atwater, H. A.; de Dood, M. J. A. Photoluminescence Quantum Efficiency of Dense Silicon Nanocrystal Ensembles in SiO_2. *Phys. Rev. B: Condens. Matter Mater. Phys.* **2006**, *73*, 132302.
(49) Valenta, J.; Juhasz, R.; Linnros, J. Photoluminescence from Single Silicon Quantum Dots at Room Temperature. *J. Lumin.* **2002**, *98*, 15−22.
(50) Bruhn, B.; Valenta, J.; Sangghaleh, F.; Linnros, J. Blinking Statistics of Silicon Quantum Dots. *Nano Lett.* **2011**, *11*, 5574−5580.
(51) Mahler, B.; Spinicelli, P.; Buil, S.; Quelin, X.; Hermier, J.-P.; Dubertret, B. Towards Non-Blinking Colloidal Quantum Dots. *Nat. Mater.* **2008**, *7*, 659−664.
(52) Gómez, D. E.; van Embden, J.; Jasieniak, J.; Smith, T. A.; Mulvaney, P. Blinking and Surface Chemistry of Single CdSe Nanocrystals. *Small* **2006**, *2*, 204−208.
(53) Tu, C.-C.; Chou, Y.-N.; Hung, H.-C.; Wu, J.; Jiang, S.; Lin, L. Y. Fluorescent Porous Silicon Biological Probes with High Quantum Efficiency and Stability. *Opt. Express* **2014**, *22*, 29996.
(54) Urbach, H. P.; Rikken, G. L. J. A. Spontaneous Emission from a Dielectric Slab. *Phys. Rev. A: At., Mol., Opt. Phys.* **1998**, *57*, 3913−3930.
(55) Novotny, L.; Hecht, B. *Principles of Nano-Optics*; Cambridge University Press: New York, 2012.

DOI: 10.1021/acsphotonics.7b01624
ACS Photonics 2018, 5, 2129−2136